Iranian Journal of Basic Medical Sciences
ijbms.mums.ac.ir

Modular 3D culture platform combining methylcellulose, testicular ECM, and Sertoli cells for *in vitro* spermatogenesis

Narjes Feizollahi [1], Ehsan Heidarian [2], Mehdi Forouzesh [3], Maryam Salem [4, 5], Soheil Kianirad [6], Nasrin Ghanami Gashti [7], Masoome Jabarpour [8], Rasool Setareyi [9], Ayob Jabari [10, 11], Farnaz Khadivi [12, 13], Morteza Koruji [14, 15], Mohammad Naji [2]*, Mehdi Abbasi [1]*

[1] Department of Anatomy, School of Medicine, Tehran University of Medical Sciences, Tehran, Iran
[2] Urology and Nephrology Research Center, Research Institute for Urology and Nephrology, Shahid Beheshti University of Medical Sciences, Tehran, Iran
[3] Legal Medicine Research Center, Legal Medicine Organization, Tehran, Iran
[4] Research Laboratory for Embryology and Stem Cells, Department of Anatomical Sciences, School of Medicine, Ardabil University of Medical Sciences, Ardabil, Iran
[5] Infertility Department, Alavi Hospital, Ardabil University of Medical Science, Ardabil, Iran
[6] Department of Chemical and Petroleum Engineering, Sharif University of Technology, Tehran, Iran
[7] Bernal Institute and School of Engineering, University of Limerick, Limerick, Ireland
[8] Department of Infertility, Shariati Hospital, Tehran University of Medical Sciences, Tehran, Iran
[9] Department of Life Science Engineering, Faculty of New Science and Technology, University of Tehran, Tehran, Iran
[10] Department of Obstetrics and Gynecology, Molud Infertility Treatment Center, Zahedan University of Medical Sciences, Zahedan, Iran
[11] Clinical Immunology Research Center, Zahedan University of Medical Sciences, Zahedan, Iran
[12] Department of Anatomy, School of Medicine, Shahrekord University of Medical Sciences, Shahrekord, Iran
[13] Medical Plants Research Center, Basic Health Sciences Institute, Shahrekord University of Medical Sciences, Shahrekord, Iran
[14] Stem Cell and Regenerative Medicine Research Center, Iran University of Medical Sciences, Tehran, Iran
[15] Department of Anatomy, School of Medicine, Iran University of Medical Sciences, Tehran, Iran

ARTICLE INFO

Article type:
Original

Article history:
Received: Dec 22, 2025
Accepted: May 18, 2026

Keywords:
Cell differentiation
Decellularized extracellular - matrix
Hydrogels
Methylcellulose
Sertoli cells
Germline adult stem cells

ABSTRACT

Objective(s): We aimed to develop and characterize a 3D culture platform combining methylcellulose (MC) with decellularized testicular extracellular matrix (ECM) and Sertoli cell co-culture to support human spermatogonial stem cell (SSC) survival and differentiation.

Materials and Methods: Human testicular cells were isolated and characterized by immunofluorescence and flow cytometry. Sheep testicular tissue was decellularized using detergents and characterized by several histology techniques. ECM was solubilized and mixed with MC at various ratios to make hybrid hydrogels. Hydrogels were characterized for pore size, porosity, mechanical properties, gelation kinetics, and degradation kinetics using scanning electron microscopy, rheological analysis, turbidity analysis, and mass loss assays. Human SSCs and Sertoli cells were cultured in 3D hydrogels for four weeks under differentiation conditions. Cell viability was assessed using the MTT assay, and gene expression of SSC, meiotic, post-meiotic, and apoptotic markers was evaluated by RT-PCR.

Results: After four weeks of proliferation, PLZF-positive cells increased from 19% to 73%. Decellularization reduced DNA content by 96% while preserving key matrix components. Hybrid hydrogels displayed interconnected porous structures with pore sizes of about 65–181 µm. All functional hydrogels supported cell viability; however, ECM-rich hydrogels significantly up-regulated PRM2 compared to 2D controls, indicating enhanced post-meiotic differentiation. MC-only scaffolds displayed elevated pro-apoptotic BAX expression compared to ECM-rich matrices, suggesting that bioactive ECM ligands confer cytoprotection.

Conclusion: The modular MC/ECM hybrid hydrogel provides a tunable, physiologically relevant 3D culture system that is superior to conventional approaches in supporting SSC maintenance and differentiation, offering promise for fertility preservation strategies.

▶ Please cite this article as:
Feizollahi N, Heidarian E, Forouzesh M, Salem M, Kianirad S, Ghanami Gashti N, Jabarpour M, Setareyi R, Jabari A, Khadivi F, Koruji M, Naji M, Abbasi M. Modular 3D culture platform combining methylcellulose, testicular ECM, and Sertoli cells for *in vitro* spermatogenesis. Iran J Basic Med Sci 2026; 29:

Introduction

In recent decades, due to the enhanced prevalence of cancers in human societies and the increasing use of treatment methods such as radiotherapy and chemotherapy, the population of patients suffering from complex reproductive disorders has increased (1). The sensitivity

***Corresponding authors:** Mohammad Naji. Urology and Nephrology Research Center, Research Institute for Urology and Nephrology, Shahid Beheshti University of Medical Sciences, Tehran, Iran. Email: mohammadnaji@sbmu.ac.ir; Mehdi Abbasi. Department of Anatomy, School of Medicine, Tehran University of Medical Sciences, Tehran, Iran. Email: abbasima@tums.ac.ir

of spermatogonial stem cells (SSCs) to cytotoxic drugs has been confirmed (2). The toxic effects of cancer treatments on reproductive function and infertility are among the most critical challenges and concerns for reproductive medicine and researchers in this field (1). Given that azoospermia occurs in adulthood in approximately 30% of boys treated for malignant diseases, bone marrow transplantation, oncological treatments, and anticancer drugs (2), researchers have sought to establish an *in vitro* spermatogenesis system (3), i.e., the differentiation of sperm from SSC during puberty, using frozen testicular tissues *in vitro* (4, 5). Several studies have been performed using 2D and 3D cultures, which have shown diverse results for spermatogenesis from SSCs to spermatozoa (6, 7). In this regard, 2D cultures, which have shown low efficiency in *in vitro* spermatogenesis, have provided valuable information on the key requirements for spermatogenesis, the main aspects controlling the differentiation and proliferation of SSCs, the factors influencing the differentiation of SSCs into spermatozoa, and the key components of spermatogenesis. However, most of these cultures neither complete spermatogenesis nor provide the same optimal conditions as the SSC niche offers to complete spermatogenesis and form sperm (8). Recent progress in tissue culture has established that *in vitro* spermatogenesis requires the maintenance of native 3D architecture and cellular organization found in seminiferous tubules.

In recent years, the limitations of traditional 2D culture have driven the development of various 3D hydrogel-based platforms designed to recapitulate the seminiferous tubule microenvironment that 2D systems cannot achieve (7, 9, 10). Early approaches utilizing synthetic scaffolds or simple hydrogels, such as alginate, agarose, or methylcellulose (MC), established the feasibility of long-term 2D culture for SSC maintenance. Nevertheless, these hydrogels suffer from lack of ligands and cell surface interactions and being biologically inactive (11, 12). In comparison to 2D cultures that used culture dishes covered with a slim layer of gelatin, collagen, Matrigel, or other extracellular matrix components, in 3D cultures with the soft agar culture system (SACS) (13) or MC (14), cells are embedded in a thick layer of gel, which provides the required conditions for the process of spermatogenesis and the production of morphological sperm (6). Abofoul-Azab *et al*., using the MC culture system, observed sperm-like cells in testicular cell cultures from immature boys during chemotherapy (15). On the other hand, natural protein-based hydrogels are highly supported through interaction with cell surface receptors, leading to biological instruction for differentiation; however, they do not have long-term efficacy in *in vitro* conditions due to enzymatic digestion over time (16). Subsequently, the field has shifted toward the use of decellularized testicular matrix (DTM) scaffolds, which better mimic the native architecture and provide essential biomechanical and biochemical cues for germ cell attachment, proliferation, and spermatogenic progression (17-19). Recent studies have further demonstrated that hybrid hydrogels, which combine the mechanical stability of synthetic polymers with the bioactive ligands present in tissue-specific ECM, represent a superior strategy for creating stable, physiologically relevant niches that support efficient *in vitro* spermatogenesis. To optimize MC for cell culture applications, it can be mixed with ECM (20-22). The ECM includes molecules such as collagen, elastin, proteoglycans, glycoproteins, and glycosaminoglycans, cytokines, and various enzymes that are crucial for intracellular communication, cell growth, and stem cell fate by producing signals that affect morphogenesis (23, 24). MC hydrogel exhibits a remarkable change in water affinity with varying temperatures, enhancing its appeal as an ideal substrate for innovative applications in cell sheet engineering (25, 26).

In addition, Sertoli cells have FSH and testosterone receptors. They are the only somatic cells that have a close relationship with germ cells and are vital for their survival and proliferation by secreting factors such as actin, stem cell factor (SCF), insulin-like growth factor-1 (IGF-1), transforming growth factor-beta, and leukemia inhibitory factor (LIF) (27, 28). Another critical factor secreted by these cells is glial cell-derived neurotrophic factor (GDNF), which, when bound to its receptor on the surface of spermatogonial cells, is crucial for coordinating the self-renewal process and growth of spermatogonial cells (29, 30). In the present study, we aimed to develop a modular 3D culture platform by combining MC with decellularized testicular ECM and Sertoli cell co-culture to better mimic the native SSC niche. The novelty of this work lies in the systematic design and characterization of hybrid MC/ECM hydrogels with different ratios, allowing us to balance mechanical stability, gelation behavior, and tissue-specific bioactivity. To our knowledge, this is among the first studies to comprehensively evaluate the structural, rheological, and biological performance of a hybrid testis-specific hydrogel system to support human SSC survival and differentiation.

Materials and Methods

Collection of human testicular tissues

Human testes were collected from six brain-dead donors aged 15-50 years from Sina University Hospital, affiliated with Tehran University of Medical Sciences (Tehran, Iran). Then, the tissues were transported on ice and held in the tissue bags containing phosphate-buffered saline (PBS; Biowest, France) and 100 U/ml pen/strep (Biowest, France). The patients' families signed informed consent forms to donate testicular tissue for research. All methods were conducted in accordance with the guidelines of the Ethical Committee of the Tehran University of Medical Sciences (IR.TUMS.MediCINE.REC.1399.707).

Testicular cell isolation and culture

Based on our previously established protocol (31), human testicular cells were isolated using a two-step enzymatic digestion. The testes were washed with PBS containing 100 U/ml pen/strep, and the testicular capsule was then detached. The tissues were treated with the first digestion solution, which was composed of DMEM containing antibiotics, 1 mg/ ml collagenase type I (Gibco, Life Technologies, Grand Island, NY, USA), 1 mg/ml hyaluronidase (Sigma-Aldrich, USA), 1 mg/ml trypsin (Sigma-Aldrich, USA), and 0.05 mg/ml Dnase (Sigma-Aldrich, USA) for 10 min at 37 °C in a shaker incubator. Then, the fragmented testicular tissues were centrifuged at 1100 rpm for 5 min. The second enzymatic digestion was performed similarly to the first step, after washing with DMEM. In the next step, the cell suspension was filtered through a 40 µm cell strainer and washed with PBS; the hemocytometer was then used to count cells. Cell viability was assessed using a 0.04% trypan blue solution (Sigma-Aldrich, USA). As Sertoli cells adhere to the culture plate more readily than SSCs, SSCs were

separated from somatic cells using the differential plating culture technique. Finally, after an overnight culture, the supernatant was collected and centrifuged at 1000 rpm for 5 min to isolate the floating cells, and then plated in a new cell culture flask.

A proliferation medium consisting of DMEM/F-12 supplemented with 5% fetal bovine serum (FBS; Biowest, France), 5% knockout serum substitute (KSR, Thermo Scientific, USA), 100 IU/ml pen/strep, 20 ng/ml glial-derived nerve growth factor (GDNF; Sigma-Aldrich, USA), and 10 ng/ml leukemia inhibitory factor (LIF; Sigma-Aldrich, USA) was used. The cells were then maintained for 4 weeks at 35 °C in a humidified atmosphere of 5% CO2. The culture medium was changed every three days, and an inverted microscope (CKX41, Olympus, Japan) was used for evaluation.

Identification of cultured cells using immunofluorescence

The expression of SSC and Sertoli-specific proteins was evaluated using immunofluorescence for GFRA1, PLZF (pre-meiotic), SCP3 (meiotic), PRM2 (post-meiotic), and Vimentin (Sertoli cells). After being washed twice with PBS, all samples were fixed with 4% paraformaldehyde (Merck KGaA, Darmstadt, Germany) at room temperature for 30 min, then permeabilized with 0.5% Triton X-100 for 30 min. After washing with PBS, 10% goat serum (Sigma-Aldrich, USA) was used to prevent nonspecific binding sites. After that, primary antibodies, including anti-PLZF, anti-GFRA1, anti-SCP3, anti-PRM2, and anti-Vimentin (Abcam, Cambridge, MA, USA), were added to the testicular cells and incubated for an additional night at 4 °C. Then, to detect the primary antibody binding sites, for two hr at room temperature, secondary antibodies labeled with FITC or PE (anti-mouse (PE), 1:200, Sigma Aldrich, St. Louis, MO, USA, and anti-rabbit (FITC), 1:200) were used. Primary antibodies were removed from the negative control sample. Following counterstaining with 4,6-diamidino-2-phenylindole (DAPI; 1 µg/mL; Sigma-Aldrich, St. Louis, MO, USA), the cells were examined under a BX51 fluorescence microscope (Olympus, Tokyo, Japan).

Flow cytometry analysis

The expression of PLZF marker was evaluated by flow cytometry after four weeks of 2D culture to evaluate the purity of SSCs after the enzymatic digestion of the testis. Permeabilization with 0.4% Triton X-100 (Sigma-Aldrich, USA) was done after fixation of SSCs with 4% paraformaldehyde. Next, about 10 µl of primary antibody (anti-PLZF antibody, 1:100, Abcam, Cambridge, MA, USA) was added to the cell suspension and incubated for 1 hr at room temperature. After washing cells with PBS, about 10 µl of secondary antibody (Abcam, Cambridge, MA, USA) conjugated with fluorescein isothiocyanate (FITC) was added for 1 hr at 4 °C. FITC-positive cells were assessed by flow cytometry (Beckman Coulter, Krefeld, Germany) and analyzed by Flowjo 7.6.1. software.

Decellularization of Sheep testicular tissue

Sheep testicular tissue was collected from a local slaughterhouse and transferred to the laboratory in PBS and antibiotics at 4 °C, then decapsulated and stored at -80 °C for 48 hr. The whole testes were cut into 1 mm diameter sections and decellularized in 0.3% (v/v) sodium dodecyl sulfate (SDS, Sigma-Aldrich, USA) in distilled water for 24 hr with ten changes and then in 1% (v/v) Triton X-100 for 6 hr with two changes on an orbital shaker (70 rpm) at room temperature. Afterward, the tissues were washed ten times for 24 hr with PBS on ice using an orbital shaker (100 rpm) to eliminate the detergents (32).

Characterization of decellularized ECM

The testicular tissues were fixed in 10% formalin solution for 24 hr and then processed and embedded in paraffin and sectioned at a thickness of five µm. Then, DAPI (Sigma-Aldrich, USA) and hematoxylin-eosin (H&E) staining were used to evaluate the quality of the decellularization process and the residual cell nuclei. Masson trichrome, Orcein, and Alcian blue staining were used to verify the collagen, elastin, and glycosaminoglycan (GAGs) contents. Microscopic observation was performed using an Olympus BX51 microscope (Olympus BX51, equipped with a DP72 digital camera, Japan).

On the other hand, for the quantitative analysis of DNA content from dried native and decellularized ECM, a DNA extraction kit (General Biological Corporation) was used. The overall DNA concentration was determined using a NanoDrop spectrophotometer (Biochrom) at 260 nm.

Preparation of MC solution

A 3.34% MC solution (Sigma, USA) was prepared according to the dispersion method, the hot-cold technique. Briefly, MC powder was gently stirred in hot deionized water (above 80 °C) to disperse gradually in 1/3 of the intended volume. Cold water was added for the remaining volume and stirred at 4 °C for 24 h. The solution was then autoclaved for 16 min and stored at -20 °C. Using this stock solution, a working concentration of MC was made, and 10X PBS or 10X DMEM/F12 was used for final adjustment of salt concentration.

Preparation of hybrid hydrogels

To create a hydrogel from ECM, decellularized ECM was powdered in liquid nitrogen and solubilized in 0.1 M HCl containing pepsin (1 mg per 10 mg of ECM) for 48 hr at 4 °C. For making the ECM pre-gel (10 mg/ml), the solubilized ECM was neutralized by NaOH (1 M, 1/10 volume of solubilized ECM), and the salt concentration was adjusted by 10X PBS (1/9 volume of solubilized ECM), and the remaining volume was compensated by 1X PBS. For cell culture experiments, 10X PBS and 1X PBS were replaced by 10X DMEM/F12 and DMEM/F12, respectively. Pre-gels of MC and ECM were mixed in different ratios for preparing hybrid hydrogels according to Table 1. Over-solubilized ECM hydrogel (SE) was prepared by solubilizing ECM with pepsin for 72 hr at RT. Then, the mixture was neutralized and freeze-dried. For the preparation of SE hydrogel, the solubilized ECM was dissolved in PBS or DMEM/F12.

Physical and mechanical characterization of hydrogels

Scanning electron microscopy (SEM)

SEM was conducted to assess the structure of hydrogels. Hydrogels were freeze-dried for 24 hr and then covered with a gold-palladium coating. Then, micrographs were captured using SU3500 SEM (Hitachi, Japan). Pore size was determined from SEM micrographs using ImageJ software. All visible pores within each analyzed SEM field were automatically selected, their areas were measured, and the Feret diameter was used as the pore-size parameter.

Table 1. Composition of hydrogels

Hydrogel code	MC pre-gel (1.26%)	MC pre-gel (1%)	ECM pre-gel (10 mg/ml)	S.ECM (25 mg/ml)	Methylcellulose: ECM ratio
M1	1000	-	-	-	100:0
M2	-	750	250	-	75:25
M3	-	500	500	-	50:50
M4	-	250	750	-	25:75
ECM	-	-	1000	-	0:100
SE	-	-	-	1000	0:100

MC: Methylcellulose; ECM: Extracellular matrix; SE: Over-solubilized ECM

Hydrogels' porosity

A liquid displacement method was performed to analyze scaffold porosity (33). Each synthesized hydrogel was lyophilized and weighed (W0). The dried scaffolds were placed into absolute ethanol and then weighed (We). The scaffold porosity was calculated according to the following formula, where Vs is the volume of the freeze-dried sample, and ρ is the density of absolute ethanol.

$$\text{Porosity (\%)} = (We-W0)/Vs\times \rho \text{ ethanol} \times 100 \quad \text{Equation 1}$$

Degradation test

To evaluate the degradation rate, hydrogels were first weighed (W0) and incubated in 10 ml PBS (pH 7.4) at 37 °C for up to 4 weeks. At the end of each week, the hydrogels were weighed after removal of excess water (Ws). Degradation rates were measured by calculating the mass loss using the following formula (34). This test was not applicable to MC and SE hydrogels. In addition, owing to the physical properties of the M2 hydrogel, it was not possible to continue testing beyond the first week.

$$\text{Mass loss (\%)} = (W0-Ws)/W0 \times 100 \quad \text{Equation 2}$$

Turbidity measurement

The gelation kinetics of hydrogels were measured by evaluating turbidity (35). The hydrogels were prepared as previously described, and the absorbance at 405 nm was measured every 2 min for 90 min. The curves were plotted using MATLAB software, and an exponential model was used for curve fitting using the following equation:

$$f(t) = a^*\exp(b^*t) + c^*\exp(d^*t) \quad \text{Equation 3}$$

Where a, b, c, and d are constant values that were achieved after curve fitting; t is time in minutes, and f(t) is absorbance. Finally, t_{lag}, $t_{1/2}$, t_{95}, and S (slope) were calculated from the mathematical model.

Rheological measurement

To assess the mechanical characteristics, gelation, and viscosity of the hydrogels, a temperature sweep test was conducted. The pre-gel samples were prepared at 4 °C as previously described. The temperature range for the test was set from 10 °C to 40 °C, with 300 measurement points. For MC, the temperature was increased to 60 °C to reach the gelation point. Approximately 2–3 ml of each pre-gel solution was placed on the parallel plates of a rheometer (Physica MCR 300, Anton Paar GmbH, Austria) with a plate diameter of 25 mm and a gap of 1 mm. Following a 5-min equilibration period at the starting temperature, measurements were performed at a constant frequency of 1 Hz and a strain amplitude of 4%. The thermal response of the hydrogels was then recorded as the temperature was gradually increased from 10 °C to 40 °C.

3D culture of testicular cells in hydrogels

After 2D culture, cells were utilized to assess differentiation and viability in six groups. Five groups of hydrogels were used for differentiation culture (M1, M3, M4, ECM, and SE) except for M2, which was not functional as a hybrid hydrogel. The culture of SSCs was performed with the density of 3×10^5 cells for each hydrogel (6×10^5 /ml) (10×10^4 cells were cultured in M1 and SE groups, 2×10^5/ml) in 24-well plates for 4 weeks. The differentiation medium was composed of DMEM/F12 medium supplemented with 10^{-7} M testosterone (Sigma-Aldrich, USA), 10^{-6} M retinoic acid (R2625, Sigma-Aldrich, USA), 2.5×10^{-5} U follicle-stimulating hormone (FSH, Gonal-F, Merck), 5% FBS, 5 % KSR, 100 IU/ml penicillin, and 100 µg/ml streptomycin. The media was refreshed every 3 days. For M1 and SE groups, 50 µl of 10X media was added each week. A 2D culture of cells was used as the control group.

Viability of cells in different experimental groups

Cell viability after 2 and 4 weeks of culture in different hydrogel groups was assessed using the methylthiazolyldiphenyltetrazolium bromide (MTT) assay (Sigma-Aldrich, St. Louis, MO, USA). The proliferation medium was used for the assay, and the density of cells was 2×10^4 per well. The cultured cells were treated with 5 mg/ml of MTT solution and incubated in 5% CO_2 at 37 °C for four hr. To achieve cell lysis and dissolve the formazan crystals, 500 µl of dimethyl sulfoxide was added to each well and incubated for 30 min at 37 °C. Then, the optical density at 570 nm was measured using a microplate reader (HTX, BioTek, USA).

Real-time polymerase chain reaction

After 4 weeks of culture in different hydrogels with differentiation medium, the relative expression of GFRA1 and PLZF (SSC-specific markers), SCP3 (spermatocyte-specific marker), PRM2 (spermatid- and sperm-specific marker), Vimentin (Sertoli cell-specific marker), BAX, and BCL-2 (apoptotic markers) was assessed by real-time PCR. The RNX-plus reagent (Sinaclon, Iran) was used to extract total RNA from cells, and DNase I treatment (Thermo Scientific, Waltham, MA, USA) was performed to remove genomic DNA. Next, the purity and concentration of extracted RNA were evaluated by a spectrophotometer (Biochrom). Then, according to the manufacturer's instructions for the cDNA synthesis kit (Thermo Scientific, Waltham, MA, USA), the total RNA was converted into cDNA. The 2X RealQ Plus MasterMix Green (Ampliqon, Denmark) and Rotor-Gene

Table 2. Primer sequences for RT-PCR

Gene	Forward 5'-3'	Reverse 5'-3'
BAX	TGTCGCCCTTTTCTACTTTG	GCCCATGATGGTTCTGATC
BCL-2	TGGAGAGTGCTGAAGATTGATG	AGTCTACTTCCTCTGTGATGTTG
PLZF	AATGGCTGTGGCAAGAAGTTC	CGTTGTGCGTTCTCAGGTG
GFRA1	CTGCCTCCTCGCCTACTC	GGTCGTTCCCACTGTTGC
SCP3	GAGAGCCTATGACTTTGAGACTG	TAATGTCAACTCCAACTCCTTCC
PRM2	CTGGAAGTTAAGAGAAAGTCACC	GCTTGAGCATTTGATGTAGGG
GAPDH	GCCACATCGCTCAGACAC	GCAACAATATCCACTTTACCAGAG

RT-PCR: Reverse transcription polymerase chain reaction

Q device (Qiagen, Germany) were used for real-time PCR in 35 cycles, employing the primers listed in Table 2. Relative expressions were normalized against the expression of glyceraldehyde-3-phosphate dehydrogenase (GAPDH) as the housekeeping gene. The comparative CT ($2^{-\Delta CT}$) method was used to evaluate the relative gene expression.

Statistical analysis

Data analysis was performed using Prism software (version 6.0). The Experiments were performed in triplicate or quadruplicate. The Kruskal-Wallis, Mann-Whitney U, and Wilcoxon tests were utilized for data analysis. The data are presented as mean±standard error mean (SEM). *P*-values<0.05 were considered statistically significant.

Results

Characteristics of isolated human testicular cells

During the first week of culture, after two-step isolation of testicular cells, SSC colonies emerged as a small population of slowly proliferating cells, while Sertoli cells showed a relatively fast growth rate (Figure 1A). By week 4 of culture, the number of colonies had obviously increased, and enlarged colonies were evident. In addition, Sertoli cells enclosed the colonies, performing a supporting role (Figure 1B).

To evaluate the characteristics of isolated human testicular cells, immunofluorescence and flow cytometry were utilized to appraise the expression of specific markers. At the end of four weeks of proliferation culture, immunofluorescence findings indicated that PLZF and GFRA1 proteins were expressed clearly in most colonies (Figure 2); however, the expression of SCP3 and PRM2 proteins was not detected in SSC colonies (Figure 3). In addition, the expression of Vimentin in Sertoli cells was evident at the periphery of SSC colonies (Figure 2).

The change in the population of SSCs during proliferation co-culture over 4 weeks was evaluated by monitoring PLZF expression by flow cytometry. The number of PLZF-positive cells was about 18.95% ± 4.3 at the beginning of cell culture (day 0, after testicular tissue digestion) (Figure 4A); however, the number of PLZF-positive cells was intensely

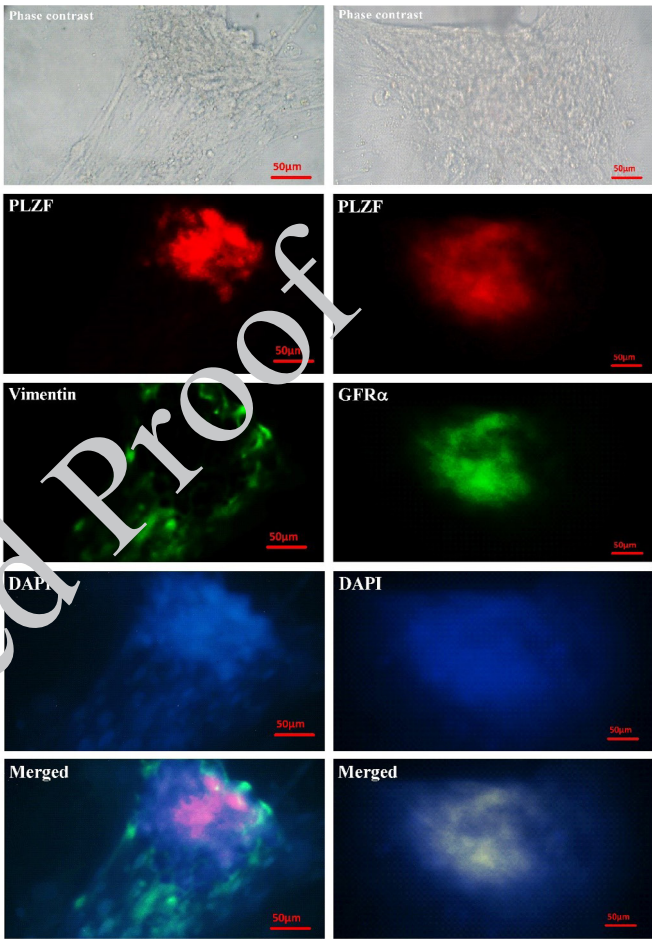

Figure 2. Expression of PLZF, GFRA1, and Vimentin proteins in 2D co-culture of human testicular cells after 4 weeks
Top row: Inverted microscope image of SSC colony with surrounding Sertoli cells. The second and third rows were stained with designated antibodies. Fourth row: counterstaining with DAPI. Lowest row: Merged images.
DAPI: 4′,6-diamidino-2-phenylindole

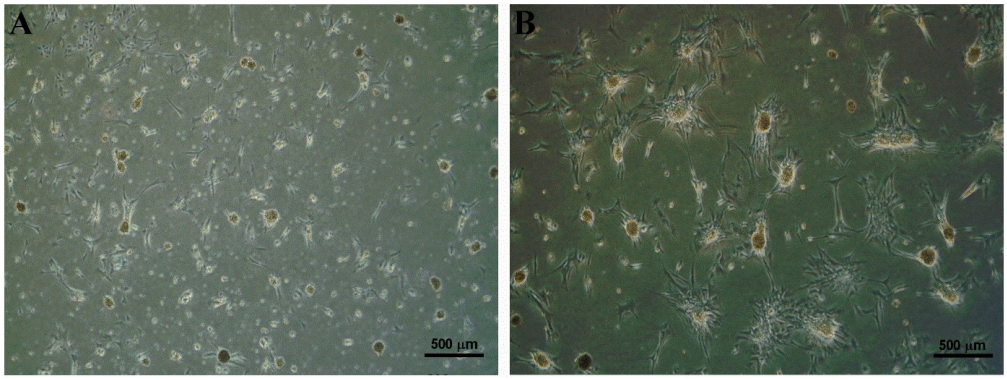

Figure 1. Inverted microscope features of testicular cells in 2D culture. Colonies of SSCs during the first week of culture (A) and four weeks after culture surrounded by Sertoli cells (B).
SSCs: Spermatogonial stem cells

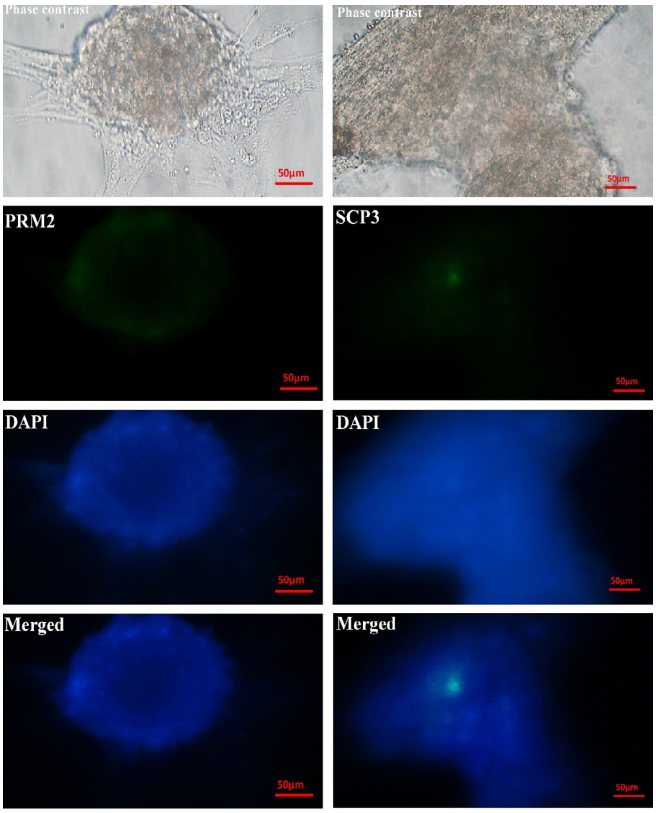

Figure 3. Expression of PRM2 and SCP3 proteins in 2D co-culture of human testicular cells after 4 weeks
Top row: Inverted microscope image of an SSC colony with surrounding Sertoli cells. The second row was stained with designated antibodies. Third row: counterstaining with DAPI. Lowest row: merged images.
DAPI: 4′,6-diamidino-2-phenylindole

increased to 72.8±0.8 after 4 weeks of proliferation co-culture (Figure 4B).

Evaluation of decellularized ECM

To evaluate the efficiency of the decellularization method in removing nuclear components, the DNA content of native and decellularized sheep testis tissues was examined. Decellularized tissue was assessed regarding remnants of cells and key structural elements by different staining methods. H&E staining showed good structural integrity in decellularized ECM and confirmed the removal of cellular elements. The preservation of collagen, glycosaminoglycans, and elastin in decellularized ECM was confirmed by Masson's trichrome, Alcian blue, and Orcein staining, respectively. Furthermore, DAPI staining demonstrated complete removal of nuclei (Figure 5A). The DNA content of native tissue (1283±32.3 ng/mg) was significantly decreased after decellularization (42.7±4.3 ng/mg) (P=0.028), which revealed about 96% decline in DNA content (Figure 5B).

Physical and mechanical characterization of hydrogels

Scanning electron microscopy (SEM) and pore features

SEM images revealed a highly interconnected porous

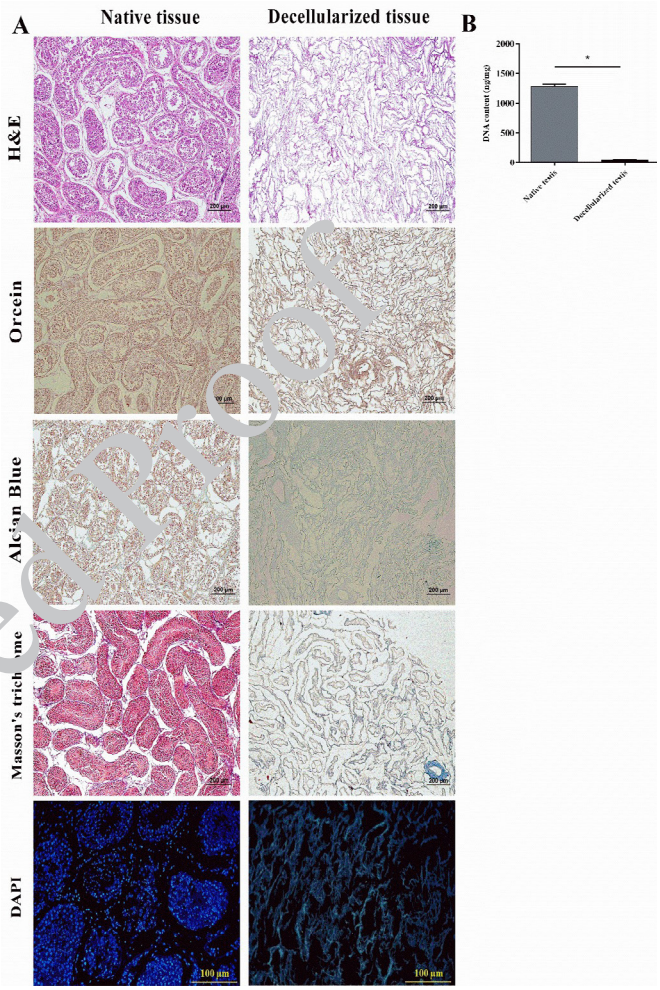

Figure 5. Evaluation of the sheep testis decellularization process
(A) Histological evaluation of native and decellularized tissues using H&E, Orcein (Elastin content), Alcian blue (GAGs content), Trichrome Massons (collagen content), and DAPI staining (nuclear components). (B) The DNA content in the native tissue and decellularized testis matrix (n = 4). *P=0.028
H&E: Hematoxylin and eosin; GAGs: Glycosaminoglycans; DAPI: 4′,6-diamidino-2-phenylindole

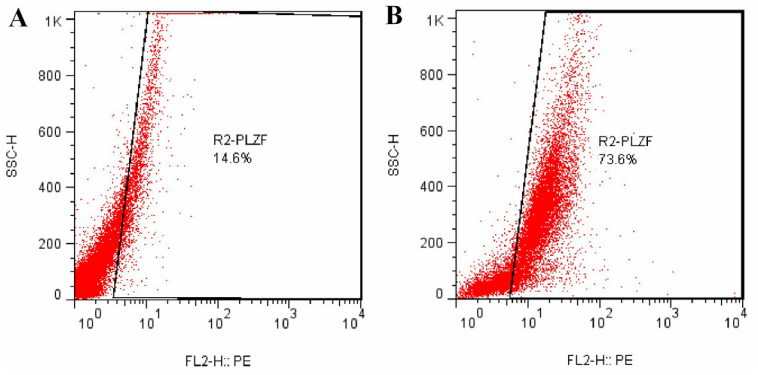

Figure 4. Flow cytometric analysis of PLZF marker expression during proliferation co-culture over 4 weeks
(A) Testicular cells after enzymatic digestion (day 0) and (B) after 4 weeks of culture.

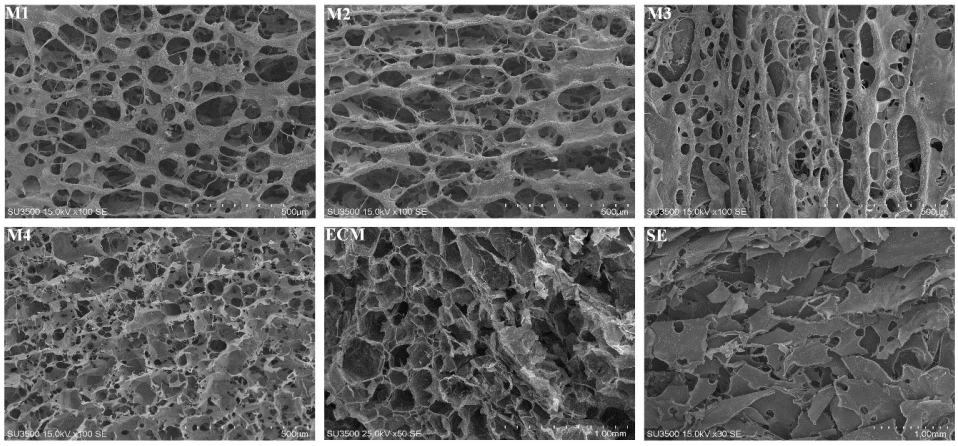

Figure 6. Scanning electron micrographs of different hydrogels
Distinct 3D architectures and pore morphologies are evident. Highly interconnected porous networks are obvious in all hydrogels except for SE. ECM hydrogels showed the largest pore size (181.6±13.3 µm), and M2 hydrogels revealed the highest level of porosity (92.01±2.1%).

structure in all hydrogel groups except for SE. SE hydrogel showed a lamellar structure with small pores (Figure 6). A gross association between morphological features (SEM images), pore size, and porosity of hydrogels was observed. ECM hydrogels showed the largest pores (181.6±13.3 µm), and this was significant compared to M1 (84.9±3.1 µm, P<0.0001), M2 (141.4±14.3 µm, P=0.005), M3 (85.08±4.7 µm, P<0.0001), and M4 hydrogels (65.6±1.8 µm, P<0.0001). The average pore size of SE hydrogel was 167.6±15.4 µm. In addition, porosity analysis showed the highest percent of porosity in M2 hydrogel (92.01±2.1%) and the lowest in SE (33.85±0.69%). The only significant difference was observed between these two hydrogels (P=0.012). The porosity in other groups was as follows: M1= 69.03±6.1%, M3=76.65±3.4%, M4=52.28±3.6%, and ECM= 84.67± 2.2%.

Degradation behavior of hydrogels

Based on our method for evaluating degradation, it was impossible to measure the degradation rate of M1, M2, and SE hydrogels. These hydrogels had a very loose structure, causing them to lose their integrity very quickly during the experiment. Therefore, it was impossible to weigh them precisely at experimental time points. In other groups, the highest rate of degradation was observed in M3 hydrogel (55.23±1.7%) at week 8 (Figure 7); however, ECM showed the lowest level of degradation (11.01±1.3%) at the end of the experiment. The degradation rate of M4 hydrogel (37.96±4.1%) was much lower than that of M3 and higher than that of ECM. The degradation rate of M3 hydrogel was significantly higher than that of ECM at all measured time points.

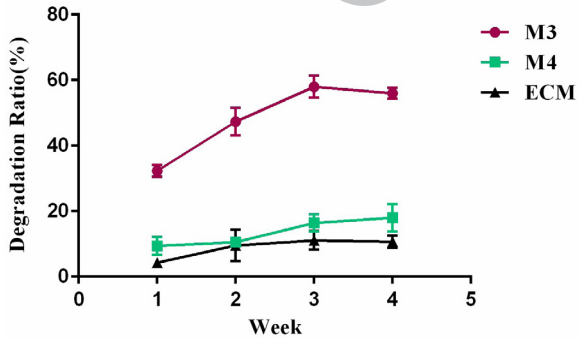

Figure 7. *In vitro* degradation profiles of hydrogels over a 4-week period
Degradation ratios (%) of the three hydrogels were measured weekly, showing a higher degradation rate for M3 compared to M4 and ECM. M4 exhibited moderate degradation, while ECM showed the slowest and most stable degradation trend (n=4). Data are presented as mean±SEM.

Turbidity

The gelation behavior of the hydrogels was examined by monitoring absorbance at 405 nm over time. All formulations exhibited the characteristic sigmoidal pattern of fibrillar network formation, comprising an initial lag phase, a rapid growth phase, and a final plateau. Despite these shared features, the timing and slope of the transitions varied among the groups.

Quantitative parameters extracted from the curves are summarized in Table 3. The ECM exhibited the shortest lag time (t_{lag}= 13.55 min), indicating the earliest onset of fibrinogenesis. The addition of MC to ECM reduced t_{lag}, with M2, M3, and M4 showing similar values (17.35, 17.75, and 17.45 min, respectively). Half-gelation time ($t_{1/2}$) followed a similar trend. ECM reached 50% gelation at 21.45 min, while the MC formulations showed slightly longer times, ranging from 23.74 to 23.94 min. The time required to reach near-complete gelation (t_{95}) again distinguished the groups. M2 required the longest duration (48.11 min), whereas ECM completed gelation faster (39.84 min). The M3 and M4 groups also approached complete gelation at times of 41.75 and 40.07 min, respectively. The slope of the growth phase (S), which reflects the rate of network development once fibril formation begins, also differed among samples. M2 displayed the lowest value (0.0295), while the M3,

Table 3. Evaluation of the turbidity in hydrogels with different concentrations of MC/ECM

	$t_{1/2}$ (min)	t_{95} (min)	S	t_{lag} (min)
M2	23.94	48.11	0.0295	17.35
M3	23.71	41.75	0.0625	17.75
M4	23.74	40.07	0.0692	17.45
ECM	21.45	39.84	0.0606	13.54

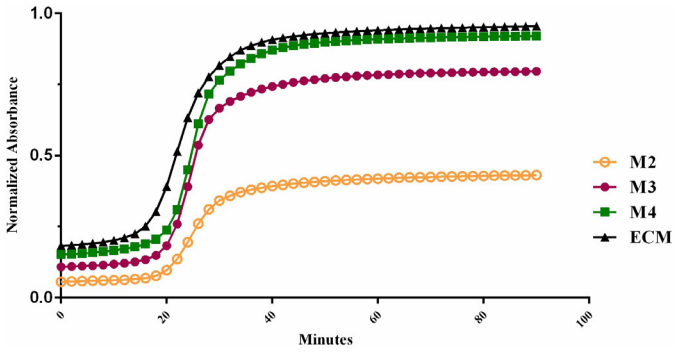

Figure 8. Gelation turbidity kinetics of ECM and MC-containing hydrogels
The sigmoidal curves illustrate the lag phase, rapid growth phase, and plateau of fibrillar network formation, with ECM showing the earliest onset of gelation and highest turbidity plateau, and increasing MC content (M2–M4) leading to delayed gelation and lower final absorbance (n = 4).
MC: Methylcellulose

M4, and ECM groups showed moderately faster growth rates (0.0625, 0.0692, and 0.0606, respectively). The final absorbance values (Figure 8) differed markedly among the formulations, with higher ECM content yielding a greater turbidity plateau, indicating a denser and more fully developed fibrillar network than in blends containing higher proportions of MC.

Rheology

A parallel-plate rheometer was used to assess the rheological characteristics of hydrogels.

Elastic and viscous properties of hydrogels were evaluated by alteration in their storage modulus (G') and loss modulus (G"), respectively. All hydrogels exhibited a higher storage modulus, indicating the dominance of the solid structure over the viscous structure. The storage modulus increased rapidly above the gelation temperature. SE hydrogel showed a minimal increase in moduli, confirming its very low potential for gel formation (Figure 9). In addition, the temperature-dependent viscosity clearly demonstrated the gelation behavior of hydrogels. The viscosity of SE hydrogel did not indicate any response to temperature rise, showing a lack of solid gel formation (Figure 10).

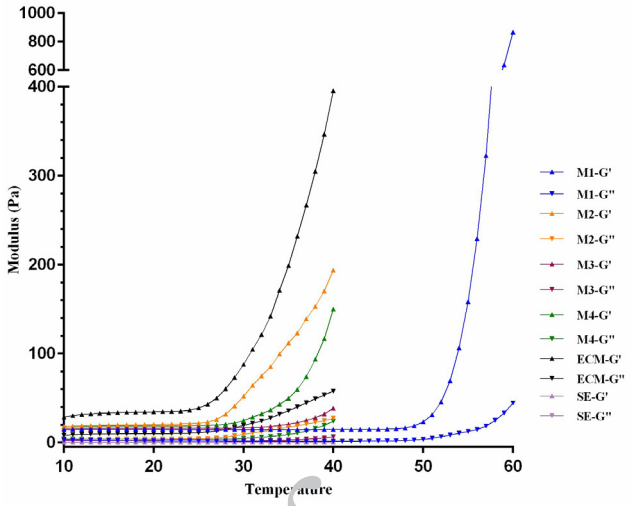

Figure 9. Temperature-dependent viscoelastic behavior of hydrogels
Storage modulus (G') and loss modulus (G") of M1, M2, M3, M4, ECM, and SE hydrogels were measured by temperature sweep using a parallel plate rheometer. Elastic responses dominated over viscous responses for all hydrogels, whereas the SE hydrogel exhibited only a slight increase in both moduli, indicating poor gel-forming ability (n=3).

Viability of cells in hydrogels

Considering the culture methods for M2, M3, M4, and ECM hydrogels, and the very unstable nature of M2 hydrogels, it was impossible to use M2 hydrogels for cell culture experiments. In all hydrogels, the viability of cultured cells was increased from week two to week four, except for the SE hydrogel, which showed a slight decline in the viability after four weeks (Figure 11). No significant changes in viability levels between different groups were noticed.

Real-time PCR analysis

We used quantitative RT-PCR to assess the expression of genes after 3D culture of cells for four weeks compared to the control group. An elevated up-regulation of BAX (apoptotic) was observed in the M1 group compared to all other groups. However, the only significant change was noticed in the M1 group compared to the M4 group (P=0.042). Regarding BCL-2 (anti-apoptotic) expression,

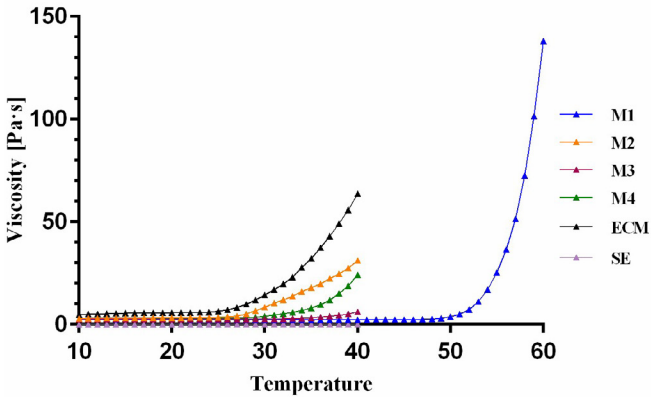

Figure 10. Temperature-dependent viscosity of hydrogels
The apparent viscosity of M1, M2, M3, M4, ECM, and SE hydrogels was monitored as a function of temperature. A sharp rise in viscosity with increasing temperature confirmed the thermoresponsive gelation of all hydrogels except for SE, whose viscosity remained nearly unchanged, indicating the absence of stable gel formation (n=3).

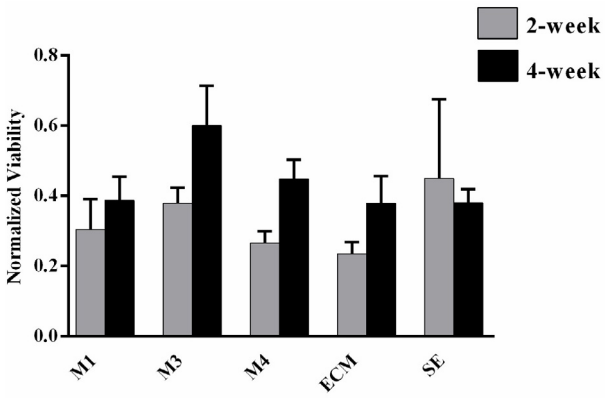

Figure 11. Viability of cells cultured in different hydrogels was assessed by comparing their metabolic activity over a 4-week period
Viability increased in all hydrogels, except for SE, after 4 weeks of culture compared with 2 weeks. No significant differences in viability levels between groups were observed (n=3). Data are presented as mean±SEM.

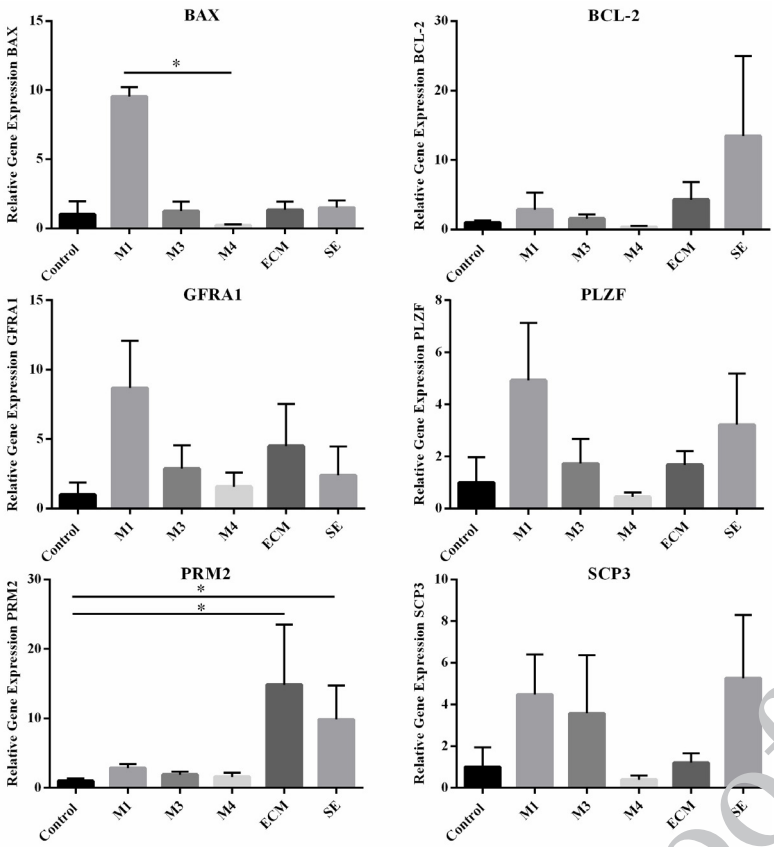

Figure 12. Relative gene expression profile of SSC- and apoptosis-related markers after 4 weeks of 3D culture in different hydrogels with differentiation induction The mRNA levels were normalized to GAPDH. A significant increase in BAX expression was detected in the M1 group compared to the M4 group. PRM2 expression was significantly higher in ECM and SE hydrogels compared to the control group (n=4). Data are presented as mean+SEM; *P<0.05
SSCs: Spermatogonial stem cells

an increase in M1, M3, ECM, and SE groups was observed, which did not reach the significance threshold. Although the expressions of GFRA1 and PLZF showed an increase in the M1 group compared to other groups, no significant pattern of expression change was noticed for these genes. ECM and SE groups showed a clear increase in PRM2 (post-meiotic) expression compared to other groups. This expression was significantly higher than the control group (P=0.02, P=0.04, respectively). SCP3 (meiotic) expression showed higher levels in the M1, M3, and SE groups; however, none of these differences were significant (Figure 12).

Discussion

The present study introduces a 3D culture platform that combines MC-based hydrogels with testis-derived ECM and Sertoli cell co-culture to support survival, maintenance, and differentiation of human SSCs. This approach addresses important limitations of conventional 2D systems, which provide valuable mechanistic insights but fail to recapitulate the complex architecture and biochemical environment of the native SSC niche and hardly achieve complete spermatogenesis (6-8). By integrating MC with tissue-specific ECM and a supportive somatic cell population, the current work contributes to the growing repertoire of 3D models aimed at *in vitro* spermatogenesis and fertility preservation in patients at risk of treatmentinduced infertility.

The two-step culture method utilized here was critical for generating an enriched SSC population before 3D encapsulation. After four weeks of proliferation co-culture, PLZF- and GFRA1-positive colonies were abundant, while meiotic (SCP3) and post-meiotic (PRM2) proteins remained undetectable, indicating that cells largely retained a pre-meiotic SSC character at this stage. This is required for controlled induction of differentiation in 3D, as premature or uncoordinated entry into meiosis can compromise the efficiency and fidelity of spermatogenesis (10). Flow cytometric analysis confirmed an increase in PLZF-positive cells from about 19% post-isolation to about 73% following expansion, reflecting the efficacy of differential plating and supplementation with GDNF and LIF, critical regulators of SSC self-renewal via GFRα1 receptor-mediated pathways (27-30). The presence of Vimentin-positive Sertoli cells at the periphery of SSC colonies further confirms maintenance of a functional somatic compartment during expansion, which is critical because Sertoli cells regulate SSC survival, self-renewal, and differentiation through structural support, metabolic coupling, and secretion of factors such as GDNF, SCF, IGF-1, transforming growth factor-beta (TGF-β), and LIF (27-30).

The decellularization protocol applied for sheep testis preserved key matrix elements while efficiently removing cellular materials, thereby generating a tissue-specific ECM suitable for hydrogel formulation. These features conformed to accepted criteria for decellularized scaffolds designed to minimize immunogenicity while maintaining biochemical and structural signals, such as integrin-mediated signaling, growth factor retention, and microarchitectural imitation,

that control cell adhesion, migration, and fate (36, 37). Earlier studies have shown that human or porcine testis ECM supports human SSC survival, Sertoli cell attachment, and functionality better than non-specific matrices, highlighting the value of organ-specific ECM in reproductive tissue engineering (24, 38). The use of sheep testis in the present work is practical in terms of availability and scalability, and existing evidence suggests that xenogeneic testis ECM can still provide a permissive environment for germ cells, although subtle species-specific compositional differences may modulate later differentiation stages (23, 24, 39).

A major novelty of our work is the creation and systematic characterization of MC/ECM hybrid hydrogels with different mixing ratios (M1, M2, M3, and M4). MC alone is mechanically stable and thermoresponsive but lacks cell-binding ligands and is biologically inert, whereas protein-based matrices such as ECM are highly bioactive but can degrade too rapidly and exhibit poor mechanical integrity under *in vitro* conditions (16, 25, 26). Combining these components aims to integrate the structural advantages of MC with the bioactivity of ECM into a single platform. SEM imaging showed that all hydrogels except SE formed highly interconnected porous architectures, with ECM hydrogels exhibiting the largest pore sizes and SE displaying lamellar structures with smaller pores. Such pore sizes (roughly 65–180 μm) and interconnectivity are compatible with diffusion of nutrients and metabolites and allow cell–cell and cell–matrix interactions that are essential for spermatogenesis (40-42). In the M1–ECM series, neither pore size nor porosity increased in a simple linear manner with increasing ECM fraction, despite the graded mixing ratios used in Table 1. This suggests that the scaffold microarchitecture was determined not only by composition but also by how MC and ECM co-assembled during gelation and subsequent freeze-drying. For example, M3 showed the highest porosity, whereas ECM had the largest pore size, indicating that intermediate MC/ECM ratios may favor a greater number of voids, while ECM-rich formulations may promote formation of fewer but larger pores. M3 and M4 showed lower pore size and porosity than expected from a simple ratio-based trend, which may reflect denser packing or partial collapse of the fibrillar network. Therefore, the structural outcome of these hybrid hydrogels is nonlinear and depends on the balance among polymer dilution, matrix self-assembly, and drying-induced pore formation, rather than on ECM percentage alone (43, 44).

Degradation analyses further explained the functional outlooks of these hydrogels. ECM alone exhibited the slowest degradation over eight weeks, whereas M3 and M4 showed progressively higher mass loss, and M1, M2, and SE could not be reliably assessed due to their very loose or unstable structures under the chosen test conditions. This highlights the classic trade-off between mechanical stability and degradability; excessively fragile scaffolds rapidly lose integrity, while persistent ones may impede necessary tissue remodeling and reorganization (45). The relatively low degradation rate of our ECM hydrogel should be interpreted in light of the assay design. In the present study, degradation was assessed using fresh hydrogels, whereas many previous reports lyophilize the scaffold before rehydration and degradation testing, potentially altering the fibrillar architecture and water-handling properties of ECM materials. Therefore, direct comparisons across studies should account for the physical state of the sample before testing. In addition, ECM degradation is highly concentration-dependent; denser ECM formulations form more stable fibrillar networks and exhibit slower mass loss, whereas lower-concentration hydrogels degrade more rapidly (46, 47). Our ECM hydrogel likely retained a compact collagen-rich architecture after gelation, which explains its relatively slow degradation compared with the MC-containing groups.

The rheological data revealed that all hydrogels except SE exhibited a storage modulus higher than the loss modulus, with a sharp increase in moduli and viscosity as temperature rose, confirming their thermoresponsive gelation and predominantly solid-like behavior. In SE, weak gel-forming ability and minimal change in viscosity indicate that extensive ECM solubilization and prolonged pepsin digestion can compromise network formation by degrading collagen fibers, thereby disrupting thermos-responsive fibrillogenesis (48). The turbidity analysis further clarifies how matrix composition governs fibrillogenesis dynamics in the MC/ECM system. ECM alone gelled fastest, as reflected by its shortest lag time and half-gelation time, indicating that native testicular matrix components efficiently nucleate and propagate fibril formation. Incorporation of MC modestly delayed gel onset and t_{95} while preserving a steep growth slope in M3–M4, suggesting that appropriate MC fractions do not severely compromise network assembly but slightly slow it, likely by diluting fibril-forming proteins. The markedly lower slope and prolonged t_{95} in M2, together with its reduced turbidity plateau, point to suboptimal network connectivity at high MC content (49). In contrast, the higher final absorbance of ECM-rich formulations indicates denser fibrillar architectures, consistent with their slower degradation and favorable support for post-meiotic differentiation, thereby linking gelation kinetics, matrix density, and biological performance in this platform.

MTT assays showed increased metabolic activity from week 2 to week 4 in all functional hydrogels (M1, M3, M4, ECM) and 2D control, with only a slight decrease in SE, and no significant differences in overall viability among groups. This indicates that under the applied hormonal and nutritional conditions, MC-rich, ECM-rich, and hybrid hydrogels are all permissive to cell viability for at least 4 weeks. The reduced viability trend in SE may be explained by its low porosity, poor gel stability, and suboptimal microarchitecture, which together could hinder diffusion and cell–matrix anchorage, promoting stress and cell death.

Gene expression analysis provides more detailed insight into how each matrix composition influences apoptosis, SSC maintenance, and progression toward later stages of spermatogenesis. M1 (pure MC) showed the highest up-regulation of the pro-apoptotic gene BAX, with a significant increase compared to M4, whereas BCL-2 (anti-apoptotic) showed non-significant increases in several 3D groups. This pattern suggests that, despite maintaining viability at the population level, an MC-only scaffold creates a more pro-apoptotic environment than ECM-rich matrices, likely owing to the lack of integrin-binding sites and other ligand-mediated signals that prevent anoikis and attenuate stress signaling (50). The lower BAX expression in M4 and ECM groups may imply that ECM incorporation exerts a cytoprotective effect, possibly via integrin engagement, sequestration, and presentation of growth factors, and a more physiological range of stiffness and viscoelasticity (16, 40, 41).

Considering germ cell markers, PLZF and GFRA1 were maintained across different hydrogels, with a trend toward higher expression in M1. It suggests that MC-only hydrogels may favor retention or expansion of undifferentiated SSCs rather than progression, especially in the presence of supportive Sertoli cells and exogenous GDNF and LIF (27, 30). This observation may be advantageous where the objective is long-term SSC maintenance and expansion rather than differentiation. In contrast, the ECM and SE groups revealed a significant increase in PRM2 expression compared to the 2D control, indicating that ECM-dominated milieus are more conducive to the acquisition of post-meiotic gene expression. Notably, PRM2 up-regulation occurred despite suboptimal physical properties of SE, reinforcing the idea that biochemical cues embedded in ECM can, to some extent, outweigh mechanical and structural limitations in inducing late spermatogenic differentiation. On the other hand, SCP3, a meiotic marker, showed higher but non-significant expression in M1, M3, and SE, indicating some degree of meiotic entry in some hydrogels; although this study may not have had sufficient power or sensitivity (e.g., single-cell resolution) to detect subtle differences in frequencies of meiotic cells between groups. The combination of significant PRM2 increases without robust changes in SCP3 suggests either asynchronous or low-frequency progression to post-meiotic states or reflects the limitation of bulk qPCR, where small but biologically relevant subpopulations can be diluted by undifferentiated or somatic cells (51).

Compared with the evolving context of 3D *in vitro* spermatogenesis models, the present platform offers several distinctive advantages. Soft agar culture systems, organotypic testis tissue cultures, alginate-based scaffolds, and hybrid agarose–laminin hydrogels have all been used to support meiotic and post-meiotic differentiation of rodent and human germ cells (6, 7, 13-15). However, many of these models either rely on intact tissue fragments with limited control over composition and geometry, or utilize generic synthetic matrices that lack testis-specific biochemical signals. By contrast, MC/ECM hydrogels provide a modular platform where the MC fraction can tune mechanical properties and gelation kinetics, and the ECM fraction provides organ-specific structural proteins and growth factors that more closely imitate the testicular niche. The ability to vary the MC:ECM ratio allows rational optimization for different goals such as SSC expansion, meiotic induction, or post-meiotic maturation, and could be further integrated with bioprinting or microfluidic technologies for spatially patterned "artificial testis" constructs (9).

Despite these advantages, our study has some limitations that point the way to future work. Bulk analyses lack the resolution to map cellular heterogeneity or organization suggestive of native seminiferous tubules, necessitating incorporation of single-cell transcriptomics and advanced 3D imaging in future work (51). The xenogeneic origin of ECM, specifically sheep, raises concerns about translation of findings and suggests the need for human ECM sourcing or xenofree alternatives to mitigate immunogenicity and enhance clinical relevance. Moreover, the study excludes other critical testis niche cells such as peritubular myoid, Leydig, and vascular cells, which contribute to hormone production, ECM remodeling, and paracrine signaling, factors essential for complete spermatogenesis *in vivo* (4).

Finally, translational considerations warrant careful attention. Any clinical use of *in vitro*–derived germ cells, particularly for prepubertal boys undergoing gonadotoxic therapy, will require rigorous demonstration of genetic and epigenetic stability, absence of malignant contamination, and long-term safety in appropriate preclinical models. Ethical and regulatory frameworks must also be taken into account, especially when xenogeneic ECM is used or when germ cells are intended for reproduction purposes.

Conclusion

In this study, we successfully developed a 3D culture platform by combining methylcellulose-based hydrogels with decellularized testicular extracellular matrix and Sertoli cell co-culture to support human SSC survival and differentiation. Systematic characterization revealed that hybrid MC/ECM hydrogels provide tunable microarchitectures with suitable porosity and interconnectivity for cell–matrix interfaces. Gene expression analysis demonstrated that ECM incorporation confers cytoprotective effects and promotes post-meiotic differentiation (with significant PRM2 up-regulation), whereas MC-only scaffolds exhibited higher pro-apoptotic signaling. The modular design enables rational optimization of MC:ECM ratios for different biological objectives, offering a versatile platform that is superior to conventional 2D systems and existing 3D models in recapitulating the testicular niche.

Acknowledgment

The authors sincerely thank the staff of the Urology and Nephrology Research Center for their invaluable support throughout this project. This work was supported by joint grants from the Research Institute for Urology and Nephrology, Shahid Beheshti University of Medical Sciences, and Tehran University of Medical Sciences, Tehran, Iran.

Authors' Contributions

N F, M S, M K, and A J designed and conceptualized the study; N F, E H, S K, and F K conducted the experiments and collected the data; M F provided human samples; N F, R S, and M J analyzed and interpreted the results; N F and N GG prepared the draft; M N and M A revised and approved the article and secured funding.

Conflicts of Interest

The authors declare no competing interests.

Declaration

This manuscript was edited with the assistance of Perplexity AI to enhance language and readability. Artificial intelligence was not used for data processing or image preparation.

References

1.Vij SC, Gilligan T. Chemotherapy and fertility. Cancer and fertility: Springer; 2016. p. 97-107.
2. Wyns C, Kanbar M, Giudice MG, Poels J. Fertility preservation for prepubertal boys: lessons learned from the past and update on remaining challenges towards clinical translation. Hum Reprod Update 2021; 27:433-459.
3. Abofoul-Azab M, Lunenfeld E, Levitas E, Zeadna A, Younis

JS, Bar-Ami S, *et al.* Identification of premeiotic, meiotic, and postmeiotic cells in testicular biopsies without sperm from Sertoli cell-only syndrome patients. Int J Mol Sci 2019; 20:470.
4. Alves-Lopes JP, Söder O, Stukenborg J-B. Testicular organoid generation by a novel *in vitro* three-layer gradient system. Biomaterials 2017; 130:76-89.
5. Baert Y, Dvorakova-Hortova K, Margaryan H, Goossens E. Mouse *in vitro* spermatogenesis on alginate-based 3D bioprinted scaffolds. Biofabrication 2019; 11:035011.
6. Stukenborg J-B, Schlatt S, Simoni M, Yeung C-H, Elhija MA, Luetjens CM, *et al.* New horizons for in vitro spermatogenesis? an update on novel three-dimensional culture systems as tools for meiotic and post-meiotic differentiation of testicular germ cells. Mol Hum Reprod 2009; 15:521-529.
7. Salem M, Khadivi F, Javanbakht P, Mojaverrostami S, Abbasi M, Feizollahi N, *et al.* Advances of three-dimensional (3D) culture systems for in vitro spermatogenesis. Stem Cell Res Ther 2023; 14:262.
8. Nguyen AV, Julian S, Weng N, Flannigan R. Advances in human In vitro spermatogenesis: A review. Mol Aspects Med 2024; 100:101320.
9. Bashiri Z, Amiri I, Gholipourmalekabadi M, Falak R, Asgari H, Maki CB, *et al.* Artificial testis: a testicular tissue extracellular matrix as a potential bio-ink for 3D printing. Biomater Sci 2021; 9:3465-3484.
10. Sun M, Yuan Q, Niu M, Wang H, Wen L, Yao C, *et al.* Efficient generation of functional haploid spermatids from human germline stem cells by three-dimensional-induced system. Cell Death Differ 2018; 25:749-766.
11. Niemczyk-Soczynska B, Gradys A, Kolbuk D, Krzton-Maziopa A, Rogujski P, Stanaszek L, *et al.* A methylcellulose/agarose hydrogel as an innovative scaffold for tissue engineering. RSC Adv 2022; 12:26882-26894.
12. Cuéllar Gaona CG, Ibarra Alonso MC, Narro Céspedes RI, Téllez Rosas MM, Reyna Martínez R, Luévanos Escareño MP. Novel studies in the designs of natural, synthetic, and compound hydrogels with biomedical applications. Revista Mexicana de Ingeniería Biomédica 2023; 44:74-96.
13. Jabari A, Gholami K, Khadivi F, Koruji M, Amidi F, Gilani MAS, *et al. In vitro* complete differentiation of human spermatogonial stem cells to morphologic spermatozoa using a hybrid hydrogel of agarose and laminin. Int J Biol Macromol 2023; 253:123801.
14. Huleihel M, Nourashrafeddin S, Plant TM. Application of three-dimensional culture systems to study mammalian spermatogenesis, with an emphasis on the rhesus monkey (Macaca mulatta). Asian J Androl 2015; 17:972-980.
15. Abofoul-Azab M, AbuMadighem A, Lunenfeld E, Kapelushnik J, Shi Q, Pinkas H, *et al.* Development of postmeiotic cells in vitro from spermatogonial cells of prepubertal cancer patients. Stem Cells Dev 2018; 27:1007-1020.
16. Gou Y, Wang A, Ding L, Yang X, Lu X, Qi Q, *et al.* A comprehensive review on protein-based hydrogels: from structure modification to applications. ChemistrySelect 2025; 10:e202405618.
17. Yang Y, Lin Q, Zhou C, Li Q, Li Z, Cao Z, *et al.* A testis-derived hydrogel as an efficient feeder-free culture platform to promote mouse spermatogonial stem cell proliferation and differentiation. Front Cell Dev Biol 2020; 8:250.
18. Di Filippo F, Brevini TAL, Pennarossa G, Gandolfi F. Generation of bovine decellularized testicular bio-scaffolds as a 3D platform for testis bioengineering. Front Bioeng Biotechnol 2024; 12:1532107.
19. Afshari F, Alaee S, Dara M, Shadi M, Chenari N, Ramezani A, *et al.* The synergic impact of decellularized testis scaffold and extracellular vesicles derived from human semen on spermatogonial stem cell survival and differentiation. Biomed Eng Online 2025; 24:94.
20. Kim EJ, Choi JS, Kim JS, Choi YC, Cho YW. Injectable and thermosensitive soluble extracellular matrix and methylcellulose hydrogels for stem cell delivery in skin wounds. Biomacromolecules 2016; 17:4-11.
21. Kim DW, Kim EJ, Kim EN, Sung MW, Kwon T-K, Cho YW, *et al.* Human adipose tissue derived extracellular matrix and methylcellulose hydrogels augments and regenerates the paralyzed vocal fold. PLoS One 2016; 11:e0165265.
22. Kim JS, Choi JS, Cho YW. Cell-free hydrogel system based on a tissue-specific extracellular matrix for in situ adipose tissue regeneration. ACS Appl Mater Interfaces 2017; 9:8581-8588.
23. Murdock MH, David S, Swinehart IT, Reing JE, Tran K, Gassei K, *et al.* Human testis extracellular matrix enhances human spermatogonial stem cell survival *in vitro*. Tissue Eng Part A 2019; 25:663-676.
24. Vermeulen M, Del Vento F, De Michele F, Poels J, Wyns C. Development of a cytocompatible scaffold from pig immature testicular tissue allowing human sertoli cell attachment, proliferation and functionality. Int J Mol Sci 2018; 19:227.
25. Contessi N, Altomare L, Filipponi A, Farè S. Thermo-responsive properties of methylcellulose hydrogels for cell sheet engineering. Mater Lett 2017; 207:157-160.
26. Forghani A, Devireddy R. Methylcellulose based thermally reversible hydrogels. Adipose-Derived Stem Cells: Methods and Protocols: Springer; 2018. p. 41-51.
27. Gao Y, Wang Z, Long Y, Yang L, Jiang Y, Ding D, *et al.* Unveiling the roles of Sertoli cells lineage differentiation in reproductive development and disorders: A review. Front Endocrinol 2024; 15:1357594.
28. Johnson J, Thompson Jr DL, Varner DD. Role of Sertoli cell number and function in regulation of spermatogenesis. Anim Reprod Sci 2008; 105:23-51.
29. Ding L-J, Yang G-J, Ge Q-Y, Yu F, Zhao X, Diao Z-Y, *et al.* FSH acts on the proliferation of type A spermatogonia via Nur77 that increases GDNF expression in the Sertoli cells. FEBS Lett 2011; 585:2437-2444.
30. Dovere L, Fera S, Grasso M, Lamberti D, Gargioli C, Muciaccia B, *et al.* The niche-derived glial cell line-derived neurotrophic factor (GDNF) induces migration of mouse spermatogonial stem/progenitor cells. PLoS One 2013; 8:e59431.
31. Salem M, Khadivi F, Feizollahi N, Khodarahmian M, Marghmaleki MS, Ayub S, *et al.* Melatonin promotes differentiation of human spermatogonial stem cells cultured on three-dimensional decellularized human testis matrix. Urol J 2024; 21:250-264.
32. Heidarian E, Naji M, Setareyi R, Shirinsokhan A, Rahimpour M, Torbati PM, *et al.* Comparing collagen and decellularized extracellular matrix in different fabrication contexts for bladder tissue engineering. J Biomed Mater Res A 2026; 114:e70015.
33. Ahmadian Z, Correia A, Hasany M, Figueiredo P, Dobakhti F, Eskandari MR, *et al.* A hydrogen-bonded extracellular matrix-mimicking bactericidal hydrogel with radical scavenging and hemostatic function for ph-responsive wound healing acceleration. Adv Healthc Mater 2021; 10:e2001122.
34. Liu Q, Dai W, Gao Y, Li S, Zhao X, Jia H, *et al.* The degradation rate of collagen-based hydrogels regulates chondrogenic differentiation of bone marrow mesenchymal stem cells. Collagen Leather 2025; 7:39.
35. Fernández-Pérez J, Ahearne M. The impact of decellularization methods on extracellular matrix derived hydrogels. Sci Rep 2019; 9:14933.
36. Saldin LT, Cramer MC, Velankar SS, White LJ, Badylak SF. Extracellular matrix hydrogels from decellularized tissues: Structure and function. Acta Biomater 2017; 49:1-15.
37. Kasravi M, Ahmadi A, Babajani A, Mazloomnejad R, Hatamnejad MR, Shariatzadeh S, *et al.* Immunogenicity of decellularized extracellular matrix scaffolds: A bottleneck in tissue engineering and regenerative medicine. Biomater Res 2023; 27:10.
38. Hashemi E, Movahedin M, Ghiaseddin A, Aghamir SMK. *In vitro* spermatogenesis on human decellularized testicular matrix plates following exosome treatment in a dynamic culture system. Stem Cell Rev Rep 2025; 21:454-465.
39. Mitchell RT, Saunders PT, Childs AJ, Cassidy-Kojima C, Anderson RA, Wallace WH, *et al.* Xenografting of human fetal testis tissue: a new approach to study fetal testis development and

germ cell differentiation. Hum Reprod 2010; 25:2405-2414.
40. Caliari SR, Burdick JA. A practical guide to hydrogels for cell culture. Nat Methods 2016; 13:405-414.
41. Rivero RE, Capella V, Liaudat AC, Bosch P, Barbero CA, Rodríguez N, *et al.* Mechanical and physicochemical behavior of a 3D hydrogel scaffold during cell growth and proliferation. RSC Adv 2020; 10:5827-5837.
42. Li H, Wijekoon A, Leipzig ND. 3D differentiation of neural stem cells in macroporous photopolymerizable hydrogel scaffolds. PLoS One 2012; 7:e48824.
43. Mukasheva F, Adilova L, Dyussenbinov A, Yernaimanova B, Abilev M, Akilbekova D. Optimizing scaffold pore size for tissue engineering: insights across various tissue types. Front Bioeng Biotechnol 2024; 12:1444986.
44. Yadav P, Beniwal G, Saxena KK. A review on pore and porosity in tissue engineering. Mater Today Proc 2021; 44:2623-2628.
45. Jeong CG, Hollister SJ. Mechanical, permeability, and degradation properties of 3D designed poly(1,8 octanediol-co-citrate) scaffolds for soft tissue engineering. J Biomed Mater Res B Appl Biomater 2010; 93:141-149.
46.Mendoza-Novelo B, Claudio-Rizo JA, Delgado J, Quintero-Ortega I, Mata-Mata J. Decellularized ECM-derived hydrogels: Modification and properties. In: Haider S, Haider A, editors. Hydrogels. London: IntechOpen; 2018.
47. Mndlovu H, Kumar P, du Toit LC, Choonara YE. A review of biomaterial degradation assessment approaches employed in the biomedical field. NPJ Mater Degrad 2024; 8:66.
48. Hofman K, Tucker N, Stanger J, Staiger M, Marshall S, Hall B. Effects of the molecular format of collagen on characteristics of electrospun fibres. J Mater Sci 2012; 47:1148-1155.
49. Ding C, Shi R, Zheng Z, Zhang M. Effect of carboxymethylcellulose on fibril formation of collagen *in vitro*. Connect Tissue Res 2018; 59:66-72.
50. Taddei ML, Giannoni E, Fiaschi T, Chiarugi P. Anoikis: an emerging hallmark in health and diseases. J Pathol 2012; 226:380-393.
51. Wang Y, Navin Nicholas E. Advances and applications of single-cell sequencing technologies. Mol Cell 2015; 58:598-609.